nature materials

LETTERS

PUBLISHED ONLINE: 31 AUGUST 2015 | DOI: 10.1038/NMAT4397

Optimal wrapping of liquid droplets with ultrathin sheets

Joseph D. Paulsen[1,2*], Vincent Démery[1*], Christian D. Santangelo[1], Thomas P. Russell[2,3,4], Benny Davidovitch[1] and Narayanan Menon[1]

Elastic sheets offer a path to encapsulating a droplet of one fluid in another that is different from that of traditional molecular or particulate surfactants[1]. In wrappings of fluids by sheets of moderate thickness with petals designed to curl into closed shapes[2,3], capillarity balances bending forces. Here, we show that, by using much thinner sheets, the constraints of this balance can be lifted to access a regime of high sheet bendability that brings three major advantages: ultrathin sheets automatically achieve optimally efficient shapes that maximize the enclosed volume of liquid for a fixed area of sheet; interfacial energies and mechanical properties of the sheet are irrelevant within this regime, thus allowing for further functionality; and complete coverage of the fluid can be achieved without special sheet designs. We propose and validate a general geometric model that captures the entire range of this new class of wrapped and partially wrapped shapes.

Elastic sheets can spontaneously wrap liquid drops in a process that has been called 'capillary origami'[2], and thus could be used to contain toxic or corrosive liquids, to sequester a delicate liquid cargo, or to shrink-wrap drops of a defined volume. An ultrathin sheet should be especially suitable for encapsulating liquids, as deformation of its naturally flat state involves only small energetic costs of bending. Because of their flexibility, ultrathin films admit small-scale structures that give the sheet new pathways for global deformation, beyond the smooth large-scale bending that occurs in thicker sheets[2–9]. We study the conformations of an ultrathin (∼100 nm) circular sheet on a drop whose volume is gradually decreased until it is completely wrapped. In this process, small-scale wrinkles and crumples[10] produce non-spherical wrappings, and large-amplitude folds finally lead to polygonal drop shapes. This sequence is counter to the intuition that a highly bendable film would simply conform to the spherical shape of a drop. Wrinkles[11–14], folds[15–17] and crumples[10,18,19] are challenging to understand on their own, let alone when they interact in a highly curved geometry. However, we show that the essence of the wrapping process can be understood without describing any small-scale features. We present a general model wherein the exposed liquid surface area is minimized, under the constraint that the sheet cannot stretch. This model explains all the observed partially and fully wrapped shapes purely geometrically, independent of material parameters, in a regime of thickness that often occurs in nature and is easily achieved in technological settings.

In our studies, a spin-coated polystyrene film with a thickness t, Young's modulus $E = 3.4$ GPa, and Poisson's ratio $\Lambda = 0.34$ was cut into a circle of radius $W = 1.52$ mm and placed on the surface of a water drop immersed in silicone oil. The sheet is characterized by a stretching modulus, $Y = Et$, and a bending modulus, $B = Et^3/[12(1-\Lambda^2)]$. The density difference between the silicone oil and the drop is $\Delta\rho = 30.2 \pm 0.8\,\mathrm{kg\,m^{-3}}$ and the interfacial tension is $\gamma = 21.8 \pm 0.5\,\mathrm{mN\,m^{-1}}$. The capillary length is $l_c = \sqrt{\gamma/\Delta\rho g} = 8.6$ mm, so gravity effects are minimal. The drop sits on a layer of high-density fluorinated oil ($\rho = 1{,}860\,\mathrm{kg\,m^{-3}}$). The volume, V, of the drop is controlled using a needle with a syringe; hereafter we refer to the effective radius $R \equiv ((3/4\pi)V)^{1/3}$.

When the volume of the drop is decreased, increasing the size ratio W/R, the sheet passes through a sequence of shapes whose side and top views are shown in Fig. 1a–d. In Fig. 1a, the sheet is decorated by radial wrinkles and stress-focusing crumples[10], but the gross shape is still axially symmetric. On decreasing the volume further, folds form around the perimeter, shown in Fig. 1b, and axisymmetry of the overall shape is broken. The drop then assumes a polygonal shape with five corners (Fig. 1c). Finally, two of these corners disappear, leaving a triangular wrapping (Fig. 1d). Figure 1e shows another triangular wrapping, using a $t = 241$ nm film. Similar progressions are found for t ranging from 29 to 394 nm, even though the bending modulus has increased by a factor of 2,500. This motivates a view of wrapping that is independent of the mechanical properties of the sheet.

When the energies of bending and stretching the sheet are both negligible, the only remaining energy relevant to the wrapped shape comes from the area A_{free} of the exposed oil–water surface. We introduce a purely geometric model in which we minimize the energy

$$U = \gamma A_{\mathrm{free}} \tag{1}$$

under the constraint that the sheet can compress but cannot stretch—that is, the distance between two points $\mathbf{x}$ and $\mathbf{y}$ of the flat disc satisfies

$$|\mathbf{f}(\mathbf{x}) - \mathbf{f}(\mathbf{y})| \leq |\mathbf{x} - \mathbf{y}| \tag{2}$$

where $\mathbf{f}$ is the gross shape that ignores local features. The distance is measured along the surface $\mathbf{f}$, which is 'submetric' to the initial flat disc[20]. The sheet (of radius W) and liquid interface enclose a volume $(4\pi/3)R^3$. The only dimensionless parameter is the size ratio W/R.

[1]Department of Physics, University of Massachusetts, Amherst, Massachusetts 01003, USA. [2]Polymer Science and Engineering Department, University of Massachusetts, Amherst, Massachusetts 01003, USA. [3]Materials Sciences Division, Lawrence Berkeley National Laboratory, Berkeley, California 94720, USA. [4]WPI—Advanced Institute for Materials Research (WPI-AIMR), Tohoku University, 2-1-1 Katahira, Aoba, Sendai 980-8577, Japan. *e-mail: paulsenj@umass.edu; vdemery@umass.edu

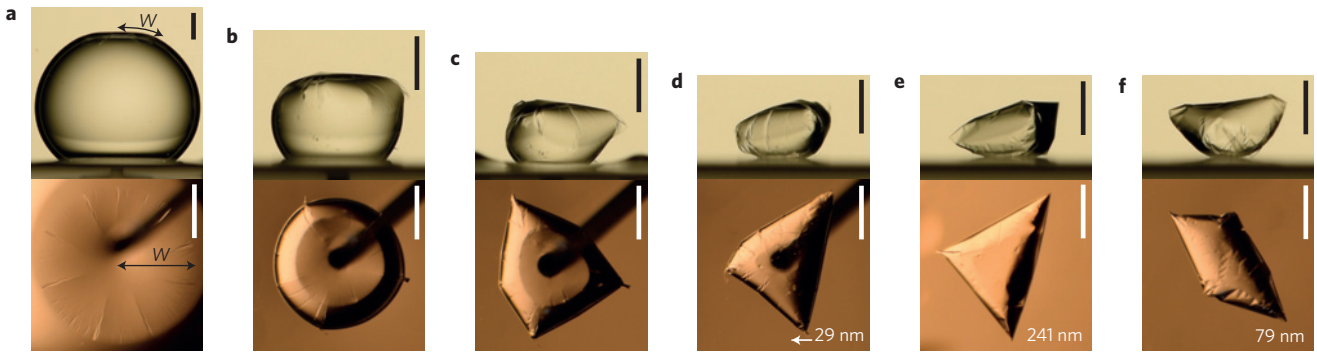

Figure 1 | Side and top views of a circular polystyrene (PS) sheet wrapping a water drop immersed in silicone oil. a–d, A PS disc of thickness $t = 29$ nm and radius $W = 1.52$ mm on a drop that is gradually shrunk. In **a**, the sheet is decorated with wrinkles and crumples. Axisymmetry of the overall shape is broken in **b**, when folds form at the perimeter of the sheet. The drop has a polygonal shape in **c** and **d**. **e**, A 241 nm sheet is also triangular at complete wrapping. **f**, A different complete wrapping shape with approximate two-fold symmetry. Scale bar, 1 mm. See also Supplementary Movies 1 and 2.

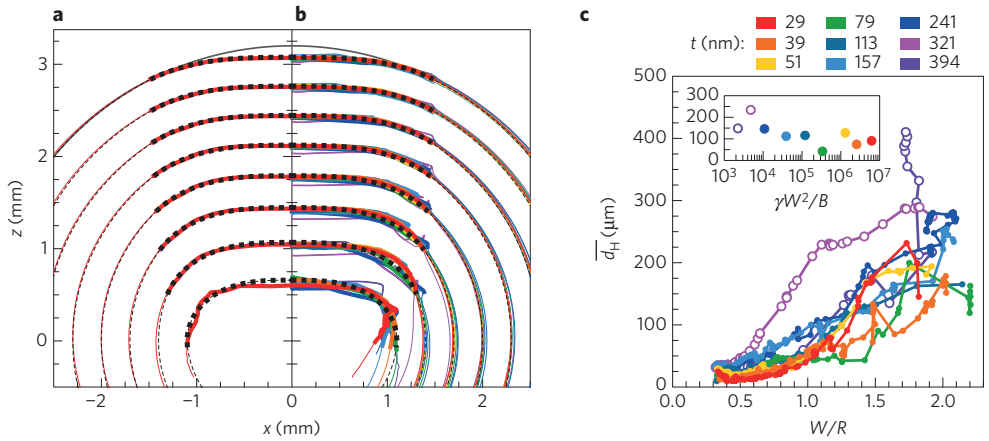

Figure 2 | Axisymmetry breaking probed by side-view profiles. a,b, Side-view profiles of wrapping for several drop sizes, for a $t = 29$ nm sheet (**a**) and for nine different thicknesses ranging from 29 to 394 nm (**b**). Solid lines: experiment. Dotted lines: analytic theory for axisymmetric wrapping with no free parameters. (For the largest drop size, a circle is also shown for comparison.) The data are described well by the axisymmetric theory for large drop size, but the profiles lose axisymmetry at small drop size. **c**, Axisymmetry breaking of the sheet, quantified by the symmetric Hausdorff distance between the experimental side-view profiles of the sheet and the analytic axisymmetric profiles, versus W/R. The Hausdorff distance between two curves X and Y, denoted $d_H(X,Y)$, is the maximum distance from a point in X to the closest point in Y; we measure $\overline{d_H}(X,Y) \equiv (1/2)d_H(X,Y) + (1/2)d_H(Y,X)$. Inset: $\overline{d_H}$ at $W/R = 1.3$, when a folding pattern is clearly established. The values are constant over a wide range of bendability, $\gamma W^2/B$, consistent with our model. Deviations from data collapse are discernible only for the thickest sheets (321 and 394 nm), marked with thinner lines in **a**,**b** and open symbols in **c**.

Neglecting the elastic energy is justified by a separation of scales between bending, surface tension and stretching:

$$\frac{B}{W^2} \ll \gamma \ll Y \tag{3}$$

In our experiments, $B/(\gamma W^2) < 5 \times 10^{-4}$ and $\gamma/Y < 3 \times 10^{-4}$. The first inequality means that the 'bendability' is large[21]: the cost for small-scale bending into wrinkles and folds is negligible. For our materials, this requires using sheets much thinner than 5 μm. We thereby depart from the regime typically probed in 'capillary origami'[2–9], wherein bending energy balances surface energy and small-scale wrinkling is not observed. The second inequality means that surface tension induces a negligible strain, so the sheet can be regarded as unstretchable. (Any polystyrene (PS) sheet that can be practically fabricated satisfies this condition at an oil–water interface.) Although the sheet is inextensible in this limit, the overall shape may be compressed by wrinkles and folds, in accord with equation (2), which gives the sheet considerable freedom to deform without stretching. This compression does not affect the area of the sheet in contact with the drop or the ambient fluid (neglecting any self-contact): only the oil–water interfacial area may change. In the limiting cases of a large drop[10] and close to complete wrapping, equation (3) may need to be modified through functions of the ratio W/R. In the case of nearly complete wrapping, the surface energy in equation (1) approaches zero; here, energy due to bending or other effects such as self-attraction or gravity could become significant.

When the gross shape is axisymmetric, our model is equivalent to the force balance of an open parachute[22] (see Supplementary Section 1). The solutions are shapes that are portions of an inflated Mylar balloon[23], which belong to the larger class of 'inflated surfaces'[20,24], where the volume contained by an unstretchable closed sheet is maximized. In Fig. 2a,b we compare the contours of this axisymmetric solution with the experimental profiles for several drop sizes and for sheet thicknesses ranging from 29 to 394 nm. For each drop, we select the theoretical curve that matches its horizontal extent; there is no free parameter in the comparison. The axisymmetric solution is in excellent agreement with experiment at large drop sizes.

As shown in Fig. 1 and also in Fig. 2a,b, the wrappings break axisymmetry for smaller drops. This deviation from the axisymmetric solution increases as the drop volume decreases, and it

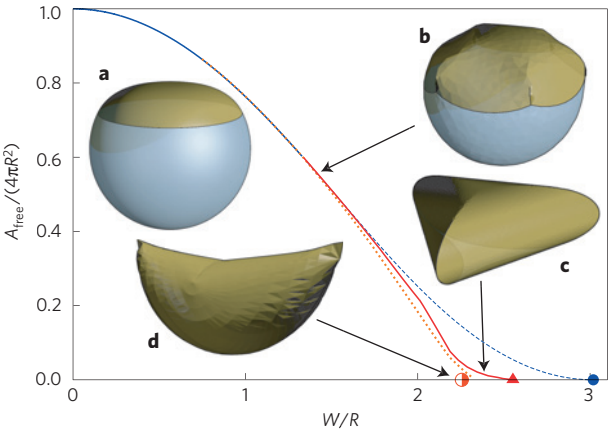

Figure 3 | Theoretical wrapping shapes and their efficiency. Normalized exposed liquid surface area $A_{free}/(4\pi R^2)$ as a function of the size ratio W/R. $A_{free}/(4\pi R^2)$ approaches 1 for large drops (that is, as $W/R \to 0$) and vanishes at a finite value of W/R, when wrapping is complete. **a**, Blue dashed line and sketch: optimal axisymmetric configuration. Closed circle: complete optimal axisymmetric wrapping. **b**, Orange dotted line and sketch: Surface Evolver simulation. **c**, Solid red line and sketch: optimal analytically determined polygonal construction. Closed triangle: complete triangular wrapping. **d**, Half-filled circle and sketch: inflated shape where two halves of the edge of the sheet are in contact.

has no trend with thickness. To show this quantitatively, Fig. 2c plots the symmetric Hausdorff distance, $\overline{d_H}$ (as defined in the caption to Fig. 2c), between the contour of the sheet and the axisymmetric shape, as a function of the size ratio W/R, for each sheet thickness.

To show that non-axisymmetric shapes can emerge from our geometric model, we numerically search for minimum-energy configurations of the model using 'Surface Evolver' (see Methods)[25]. For small W/R, the simulated shapes are consistent with the analytic axisymmetric solution. For large W/R, non-axisymmetric configurations are found with smaller exposed liquid area A_{free}. This is demonstrated in Fig. 3, which plots A_{free} normalized by the area of the bare drop, $4\pi R^2$, as a function of W/R.

We pause here to note that the breaking of axial symmetry by these ultrathin circular films is perhaps counter to intuition. One might imagine that an infinitely bendable sheet would simply conform to the spherical shape that the drop would otherwise have. Instead, geometrical constraints in the sheet lead to highly non-spherical shapes that minimize the exposed interfacial area.

The appearance of folds marks the breaking of axisymmetry in both experiment and simulation. Whereas wrinkles absorb excess azimuthal length uniformly around the sheet, folds localize excess length from a finite angular region. (Crumples, whose mechanics are not fully understood[10], do not absorb a large excess length in a small structure.) To examine folded shapes in three dimensions, we use a laser sheet to scan the topography of a fluorescently dyed PS sheet. Figure 4a shows the three-dimensional shape of a portion of the sheet for $W/R = 1.38$. Going from the edge of the sheet towards the centre, the contour lines become straighter, indicating an angular sector with predominantly radial curvature. Figure 4b shows top and side views of the drop. In Fig. 4c, we plot the height, z, of the sheet versus the radial coordinate, r. Cross-sections of the sheet halfway between two folds exhibit the same radial profile as the optimal axisymmetric wrapping. Thus, the sheet consists approximately of N 'petals' that are curved in one direction, following the parachute shape along their centrelines. These petals join together at folds.

For a complete wrapping with cross-sections that are regular N-gons (as opposed to the circular cross-sections of the axisymmetric case), the optimal midline of the curved faces corresponds to the parachute shape (see Supplementary Section 2.1). This wrapping is obtained by drawing N petals on a flat circular sheet, and curling the petals by folding away the material between them (that is, the grey regions in Fig. 4d). A construction for a partial wrapping is obtained

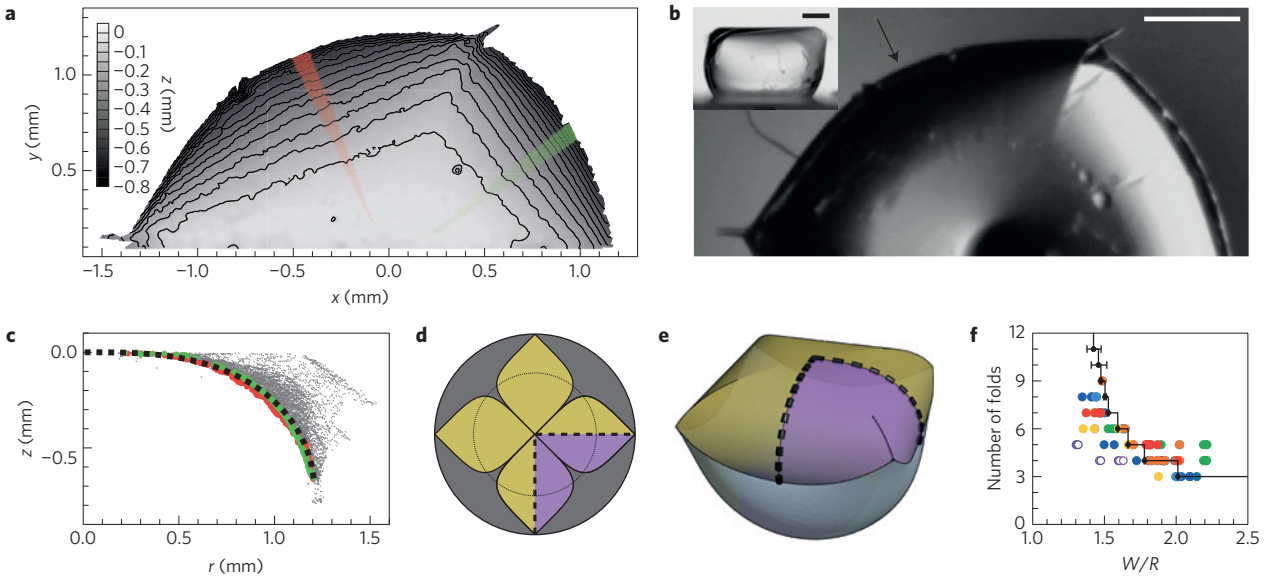

Figure 4 | Polygonal partial wrapping by petals and folds. a, Three-dimensional shape of a wrapping obtained from scanned sheet illumination, deep in the non-axisymmetric regime. A film of thickness 61 nm is prepared with Nile Red fluorescent dye and scanned with a green laser ($\lambda = 532$ nm). **b**, Top view of the wrapping in **a**. Inset: side view from the angle indicated by the arrow. Scale bar, 500 μm. **c**, Height of the sheet z versus the radial coordinate, r. Red and green points correspond to the two radial cuts highlighted in **a**. Dotted line: parachute shape. **d**, Petal shapes. The grey areas accumulate into folds. **e**, Rendered polygonal wrapping of the petal shape in **d**. **f**, Number of folds as a function of size ratio, W/R. Line: optimal number of sides in the simulation with a polygonal construction for the sheet (error bars denote the uncertainty in locations of the crossings of the computed energy curves). Coloured circles: experiment (same colour code as in Fig. 2). The thickest two sheets (321 and 394 nm, open symbols) have fewer folds, indicating the possible onset of a regime in which bending energy plays a role.

by cutting these petals with a smaller circle (as shown by the thin dotted line in Fig. 4d for $N=4$) and computing the exposed liquid surface using 'Surface Evolver' (as pictured in Figs 4e and 3c, and described in Supplementary Section 2.2). At fixed W/R, we determine the number of folds, N, that gives the lowest energy wrapping. Figure 4f shows that N decreases from large values near $W/R \simeq 1.4$, down to $N=3$ close to complete wrapping. The number of folds predicted by this construction is consistent with experiment. For $W/R \gtrsim 1.4$, the best such N-petal wrapping has a lower energy than axisymmetric wrapping, and agrees well with the full simulations of the sheet and the exposed interface, as shown in Fig. 3.

An alternative completely wrapped geometry with two-fold symmetry is sometimes seen in the experiments, as pictured in Fig. 1f. Here, two halves of the sheet's edge are in contact with each other, as for an empanada, calzone, or pierogi. Our simulations show that this wrapping is more efficient than the triangular construction for complete wrapping: it encapsulates a drop at $W/R \simeq 2.26$ instead of $W/R \simeq 2.55$. This finite difference is too large to be affected by bending or other corrections. Instead, history plays an important role in the selection of the complete wrapping configuration, because folds can shrink or grow but do not translate along the perimeter. Thus, a three-fold partial wrapping cannot reposition its folds to be equilateral, nor can it transform into an efficient two-fold complete wrapping.

The nature of the folding transition, as well as the critical value of W/R at which the axisymmetric state becomes unstable to folds, await theoretical analysis (see Supplementary Section 2.3). At small values of W/R, our experiments and simulations, as well as previous work[10], indicate that the shape is wrinkled but has no folds. As W/R is decreased from large values to $W/R \simeq 1.4$, our simulations show that the optimal number of folds increases (see Fig. 4f). This series of polygonal shapes approaches the axisymmetric shape, which suggests a possible continuous transition from the axisymmetric state.

We have witnessed how a delicate circular elastic sheet with negligible bending cost will nonetheless guide a liquid drop to a non-spherical shape. A variety of other final states can be achieved by starting with non-circular wrappers (as indicated in Supplementary Section 3, Supplementary Fig. 4 and Supplementary Movie 3, where we use a rectangular strip). We expect that elastic wrappers could also tailor the mechanical rigidity of drops. For example, our model suggests that we can achieve internal pressures that are a non-trivial function of the wrapping ratio W/R, allowing substantial suppression of the internal pressure (as indicated in Supplementary Section 1 and Supplementary Fig. 2). Although particles can also stabilize non-spherical shapes by interfacial jamming[26–28], an elastic sheet offers a route to achieving a discrete set of metastable shapes with different symmetries. This scheme is robust to spatial variations of surface chemistry, because the wrapping process does not depend on a competition of material-dependent energy scales.

Methods

Methods and any associated references are available in the online version of the paper.

Received 30 March 2015; accepted 24 July 2015; published online 31 August 2015

References

1. Binks, B. P. Particles as surfactants—similarities and differences. *Curr. Opin. Colloid Interface Sci.* **7,** 21–41 (2002).
2. Py, C. *et al.* Capillary origami: Spontaneous wrapping of a droplet with an elastic sheet. *Phys. Rev. Lett.* **98,** 156103 (2007).
3. Reis, P. M., Hure, J., Jung, S., Bush, J. W. M. & Clanet, C. Grabbing water. *Soft Matter* **6,** 5705–5708 (2010).
4. Gao, L. & McCarthy, T. J. Teflon is hydrophilic. Comments on definitions of hydrophobic, shear versus tensile hydrophobicity, and wettability characterization. *Langmuir* **24,** 9183–9188 (2008).
5. Guo, X. *et al.* Two- and three-dimensional folding of thin film single-crystalline silicon for photovoltaic power applications. *Proc. Natl Acad. Sci. USA* **106,** 20149–20154 (2009).
6. Pineirua, M., Bico, J. & Roman, B. Capillary origami controlled by an electric field. *Soft Matter* **6,** 4491–4496 (2010).
7. Chen, L., Wang, X., Wen, W. & Li, Z. Critical droplet volume for spontaneous capillary wrapping. *Appl. Phys. Lett.* **97,** 124103 (2010).
8. Antkowiak, A., Audoly, B., Josserand, C., Neukirch, S. & Rivetti, M. Instant fabrication and selection of folded structures using drop impact. *Proc. Natl Acad. Sci. USA* **108,** 10400–10404 (2011).
9. Jamin, T., Py, C. & Falcon, E. Instability of the origami of a ferrofluid drop in a magnetic field. *Phys. Rev. Lett.* **107,** 204503 (2011).
10. King, H., Schroll, R. D., Davidovitch, B. & Menon, N. Elastic sheet on a liquid drop reveals wrinkling and crumpling as distinct symmetry-breaking instabilities. *Proc. Natl Acad. Sci. USA* **109,** 9716–9720 (2012).
11. Huang, J. *et al.* Capillary wrinkling of floating thin polymer films. *Science* **317,** 650–653 (2007).
12. Schroll, R. D. *et al.* Capillary deformations of bendable films. *Phys. Rev. Lett.* **111,** 014301 (2013).
13. Chopin, J., Démery, V. & Davidovitch, B. Roadmap to the morphological instabilities of a stretched twisted ribbon. *J. Elast.* **119,** 137–189 (2015).
14. Vella, D., Huang, J., Menon, N., Russell, T. P. & Davidovitch, B. Indentation of ultrathin elastic films and the emergence of asymptotic isometry. *Phys. Rev. Lett.* **114,** 014301 (2015).
15. Pocivavsek, L. *et al.* Stress and fold localization in thin elastic membranes. *Science* **320,** 912–916 (2008).
16. Holmes, D. P. & Crosby, A. J. Draping films: A wrinkle to fold transition. *Phys. Rev. Lett.* **105,** 038303 (2010).
17. Diamant, H. & Witten, T. A. Compression induced folding of a sheet: An integrable system. *Phys. Rev. Lett.* **107,** 164302 (2011).
18. Witten, T. A. Stress focusing in elastic sheets. *Rev. Mod. Phys.* **79,** 643–675 (2007).
19. Aharoni, H. & Sharon, E. Direct observation of the temporal and spatial dynamics during crumpling. *Nature Mater.* **9,** 993–997 (2010).
20. Pak, I. & Schlenker, J.-M. Profiles of inflated surfaces. *J. Nonlin. Math. Phys.* **17,** 145–157 (2010).
21. Davidovitch, B., Schroll, R. D., Vella, D., Adda-Bedia, M. & Cerda, E. A. Prototypical model for tensional wrinkling in thin sheets. *Proc. Natl Acad. Sci. USA* **108,** 18227–18232 (2011).
22. Taylor, G. I. On the shapes of parachutes (paper written for the Advisory Committee for Aeronautics, 1919) in *The Scientific Papers of Sir Geoffrey Ingram Taylor* Vol. 3 (ed. Batchelor, G. K.) 26–37 (Cambridge Univ. Press, 1963).
23. Paulsen, W. H. What is the shape of a mylar balloon? *Am. Math. Mon.* **101,** 953–958 (1994).
24. Pak, I. Inflating the cube without stretching. *Am. Math. Mon.* **115,** 443–445 (2008).
25. Brakke, K. A. The surface evolver. *Exp. Math.* **1,** 141–165 (1992).
26. Subramaniam, A. B., Abkarian, M., Mahadevan, L. & Stone, H. A. Colloid science: Non-spherical bubbles. *Nature* **438,** 930–930 (2005).
27. Zoueshtiagh, F., Baudoin, M. & Guerrin, D. Capillary tube wetting induced by particles: Towards armoured bubbles tailoring. *Soft Matter* **10,** 9403–9412 (2014).
28. Cui, M., Emrick, T. & Russell, T. P. Stabilizing liquid drops in nonequilibrium shapes by the interfacial jamming of nanoparticles. *Science* **342,** 460–463 (2013).

Acknowledgements

We thank M. Juszkiewicz for early contributions to this work and O. Agam for helpful discussions. Funding from the W. M. Keck Foundation is gratefully acknowledged.

Author contributions

All authors contributed to designing the research and writing the manuscript; J.D.P. and V.D. performed the research; J.D.P. conducted the experiments; J.D.P., T.P.R. and N.M. analysed the experimental data, V.D., C.D.S. and B.D. conducted the analytic and numerical computations.

Additional information

Supplementary information is available in the online version of the paper. Reprints and permissions information is available online at www.nature.com/reprints. Correspondence and requests for materials should be addressed to J.D.P. or V.D.

Competing financial interests

The authors declare no competing financial interests.

Methods

Experiment. Our thin films were made by spin-coating dilute solutions of polystyrene (PS) ($M_n = 99$ k, $M_w = 105.5$ k, Polymer Source) in toluene (99.8%, Sigma-Aldrich) onto glass microscope slides ($25 \times 75 \times 1.0$ mm), following ref. 11. Film thickness was varied by changing the spinning speed (1,000–4,000 r.p.m.) or the polymer concentration (1–5% w/w). The thickness was measured using a white-light interferometer (Filmetrics F20-UV). Circular films (radius $W = 1.52$ mm) were cut near the centre of the slides, where the thickness is uniform to within 2%.

The circular film was floated onto water in a glass container having a hydrophobic surface treatment. Silicone oil (Fisher Scientific) and high-density fluorinated oil (Perfluoro-compound FC-40, Acros Organics) were then added sequentially, and the layer of water collected into a single drop. (The two oils are partially miscible and were mixed before the experiment.) Shrinking this drop through a needle allows one to tune the wrapping ratio, W/R.

In the laser scanning experiments, fluorescent dye (Nile Red, TCI America) was first dissolved into the toluene before adding the PS. A sheet of green laser light ($\lambda = 532$ nm) was scanned across the polymer sheet from above, and long-pass filters were used to image the emitted light from the polymer sheet. The three-dimensional shape of the sheet was reconstructed from simultaneous side and top views of the scan.

Numerical computations. The numerical computations were performed using the software 'Surface Evolver'[25]. We studied the behaviour of the whole model system, which consists of a sheet attached to a liquid interface. The liquid interface is given a surface tension $\gamma = 1$. The sheet, a disc of radius $W = 1$, is given a finite stretching modulus $Y = 10$ and no bending modulus ($B = 0$). In each simulation, the enclosed volume V is held constant. After minimizing the energy using the conjugate gradient algorithm, the stretching modulus is multiplied by 10 and the minimization is performed again. The process is repeated until the stretching modulus reaches 10^4.

For small volumes (that is, large W/R), the system may find a local minimum with a large number of folds. In this situation, a small random displacement is applied to all the vertices (using the jiggle command) and the minimization is performed. These steps are repeated until the system finds a steady configuration.

Variants to this scheme are used in the cases of the polygonal partial wrapping construction, and for complete wrapping. To compute the exposed liquid area for the polygonal construction for partial wrapping, the analytical polygonal shape is imposed to the sheet, and the area of the liquid interface is minimized at constant volume. To maximize the enclosed volume at complete wrapping, one must specify how the sheet is closed. In the empanada shape, two halves of the edge of the sheet are sewn together, and the enclosed volume is then maximized. The resulting shape is rendered in Fig. 3d; it encloses a volume $V \simeq 0.36W^3$ ($W/R \simeq 2.26$, half-filled circle on Fig. 3).

nature materials

SUPPLEMENTARY INFORMATION

DOI: 10.1038/NMAT4397

Optimal wrapping of liquid droplets with ultrathin sheets

Joseph D Paulsen, Vincent Démery, Christian D Santangelo,
Thomas P Russell, Benny Davidovitch, Narayanan Menon

July 23, 2015

This PDF file includes:

Supplementary Text

Captions for Movies S1 to S3

Supplementary Text:

1 Axisymmetric shape

We adapt the arguments used by Taylor to compute the shape of a parachute (*22*) to derive the shape of the sheet on a drop when it is assumed to be axisymmetric. This direct approach uses force balance arguments; a purely geometrical approach could be adapted from (*23*).

The parametrization is pictured in Fig. S1: the polar material coordinates are denoted (s, θ). The gross shape of the sheet is axisymmetric, of the form

$$\boldsymbol{X}(s,\theta) = \begin{pmatrix} r(s)\cos(\theta) \\ r(s)\sin(\theta) \\ z(s) \end{pmatrix}. \tag{1}$$

DOI: 10.1038/NMAT4397

We denote $\phi(s)$ the angle between $\boldsymbol{X}'$ and an horizontal plane, $\phi(s) = -\arctan(z'(s)/r'(s))$ (the prime denotes a derivative with respect to s). The resulting shape satisfies $r(s) < s$ for any $s > 0$, hence all the lines of latitude (i.e., circles of constant s) have a negative effective strain, namely wrinkles collapse the real strain, and the hoop stress vanishes, $\sigma_{\theta\theta} = 0$. The radial stress is $\sigma_{ss}(s)$.

An in-plane force balance in the s direction shows that $\partial_s[s\sigma_{ss}(s)] = 0$ (*10, 21*):

$$\sigma_{ss}(s) = \frac{c}{s}. \tag{2}$$

A second equation comes from a vertical force balance on a portion of the sheet $s \leq s_0$, that reads $P\pi r(s_0)^2 = 2\pi s_0 \sigma_{ss}(s_0)\sin(\phi(s_0))$, where P is the pressure in the drop. The pressure is exerted on a disc of radius $r(s_0)$, and is balanced by the radial stress exerted on the circle of latitude whose length is $2\pi s_0$. Using Eq. 2, the vertical force balance equation is

$$r(s)^2 = \frac{2c}{P}\sin(\phi(s)). \tag{3}$$

If the sheet has no radial strain, its length in the radial direction is the rest length, i.e., $|\boldsymbol{X}'(s)|^2 = r'(s)^2 + z'(s)^2 = 1$; thus $r'(s) = \cos(\phi(s))$, $z'(s) = -\sin(\phi(s))$. Differentiating Eq. 3 and using $r'(s) = \cos(\phi(s))$ leads to

$$\phi'(s)^2 = \alpha^2 \sin(\phi(s)), \tag{4}$$

with $\alpha^2 = 2P/c$. We recognize this equation as the conservation of the energy of a simple pendulum, up to the variable change $\phi = (\pi/2) - \psi$. With the boundary condition $\phi(0) = 0$ set by the regularity of the sheet at the pole, the solution is

$$\phi(s) = \frac{\pi}{2} - 2\arcsin\left(\frac{1}{\sqrt{2}}\mathrm{sn}\left(\frac{\alpha s}{\sqrt{2}} + K(1/2)\,\middle|\,\frac{1}{2}\right)\right), \tag{5}$$

where $\mathrm{sn}(x|k^2)$ is a Jacobi elliptic function and $K(k^2)$ is the complete elliptic integral (*28*); k is the elliptic modulus (here, $k = 1/\sqrt{2}$). On the exterior of the sheet the liquid surface is a

sphere of radius $R_{\rm d}$. Since we consider the sheet to have zero bending modulus, a finite angle cusp between the liquid interface and the sheet is excluded, hence $R_{\rm d} = r(W)/\sin(\phi(W))$.

For a given value of α, the volume of liquid and the free area of the liquid interface can be computed, and are shown by the blue curve in Fig. 3. Note that the pressure P and constant c are determined as functions of the volume of the drop V and the surface tension γ. Figure S2 shows the pressure P (made dimensionless by rescaling with γ/W) versus the size ratio, W/R. As the volume of the drop is reduced (increasing W/R), the pressure increases at first, and then decreases until it vanishes at complete wrapping.

From the completely wrapped shape $(r_{\rm comp}(s), z_{\rm comp}(s))$, which is defined by $r_{\rm comp}(W) = 0$, the partially wrapped shapes can be expressed through

$$r_\omega(s) = \omega^{-1} r_{\rm comp}(\omega s), \tag{6}$$

$$z_\omega(s) = \omega^{-1} r_{\rm comp}(\omega s), \tag{7}$$

where $\omega \in [0, 1]$ is the *wrapping ratio* ($\omega = 0$ is the flat state, $\omega = 1$ is the complete wrapping). This can be shown from inextensibility ($r'(s)^2 + z'(s)^2 = 1$) and Eq. 4. In the following, $r(s)$ and $z(s)$ stand for $r_\omega(s)$ and $z_\omega(s)$ for any ω, unless stated otherwise. We refer to the axisymmetric shapes given by Eqs. 6 and 7 as the "parachute" shapes (*22*).

2 Non axisymmetric states

2.1 Polygonal shape at complete wrapping

We determine the properties of regular polygonal shapes. We first address the case of complete wrapping, which is simpler. As stated in the main text, the completely wrapped configuration is selected by its volume: the larger the volume it encloses, the sooner complete wrapping occurs upon reducing the volume of the drop. This optimization problem leads to precise polygonal configurations.

DOI: 10.1038/NMAT4397

A regular polygonal shape consists of N petals rooted at the center of the disc (see Fig. 4D and E). The full shape is determined by the distance $r_N(s)$ between the vertical axis and the points of the centerline of the petals that lie at a material distance s from the origin. The horizontal cross-section containing this point is a polygon of area

$$a_N(r(s)) = N \tan\left(\frac{\pi}{N}\right) r_N(s)^2. \tag{8}$$

Denoting $z_N(s)$ the vertical position of this point, the enclosed volume is given by

$$V_N = N \tan\left(\frac{\pi}{N}\right) \int_0^W r_N(s)^2 |z'_N(s)| ds. \tag{9}$$

The only difference between this expression and the expression giving the volume of the axisymmetric shape is the prefactor of the integral, which is π for the axisymmetric shape. Note that $N \tan(\pi/N) \underset{N\to\infty}{\longrightarrow} \pi$: the axisymmetric shape can be seen as a polygonal shape whose number of sides goes to infinity.

The inextensibility constraint for the petals centerline is identical to the axisymmetric case,

$$r'_N(s)^2 + z'_N(s)^2 = 1. \tag{10}$$

Eqs. 9 and 10 define the same optimization problem for the axisymmetric shape (*23*). As a result, the petals centerline follow the parachute shape, $r_N(s) = r(s)$, $z_N(s) = z(s)$, and the volume of the N-sided complete wrapping is given by

$$V_N = \frac{N}{\pi} \tan\left(\frac{\pi}{N}\right) V_{\text{axi}}, \tag{11}$$

where V_{axi} is the volume of the axisymmetric shape. The volume is a decreasing function of N, and is thus maximal for $N = 3$.

The enclosed volume of the axisymmetric wrapping is $V_{\text{axi}} \simeq 0.15W^3$ ($W/R \simeq 3.02$), whereas the triangular shape encloses a volume $V_3 \simeq 0.25W^3$ ($W/R \simeq 2.55$).

2.2 Polygonal shape at partial wrapping

We use the polygonal shape at complete wrapping as a construction for the shape of the sheet at partial wrapping. To construct a partial polygonal wrapping, we cut a disc out of the flat petal pattern for a complete polygonal wrapping (see Fig. 4D; an example cut is shown by the dotted line). This disc is rescaled so that it has radius W. As in full wrapping, creases are made along the edges of the petals (solid lines in Fig. 4D), so that the gray portions accumulate into folded flaps. An example of the folded shape for $n = 4$ at one value of W/R is shown in Fig. 4E. The $n = 4$ flat petal pattern is reproduced in Fig. S3; the interested reader may wish to print, cut out, and fold their own wrapping from this template.

To determine the shape of the liquid interface, the edge of the sheet should be parametrized completely; this is done by writing the shape of a half of a single petal in material coordinates, which is easier using the cartesian material coordiates $(u, v) = (s\cos(\theta), s\sin(\theta))$:

$$\boldsymbol{X}_{N,\omega}(u, v) = \begin{pmatrix} r_\omega(u) \\ v \\ z_\omega(u) \end{pmatrix}, \tag{12}$$

for $0 \leq v \leq \tan(\pi/N) r_\omega(u)$. The part of the sheet such that $v > \tan(\pi/N) r(u)$ is absorbed in the fold (grey area in Fig. 4D), and has no impact on the energy of the sheet, so that we do not need to describe it. In polar coordinates, the shape reads

$$\boldsymbol{X}_{N,\omega}(s, \theta) = \begin{pmatrix} r_\omega(s\cos(\theta)) \\ s\sin(\theta) \\ z_\omega(s\cos(\theta)) \end{pmatrix}, \tag{13}$$

for $\theta \in [0, \theta^*(s)]$, where $s\sin(\theta^*(s)) = \tan(\pi/N) r_\omega(s\cos(\theta^*(s)))$. The shape for $\theta \in \left[\theta^*(s), \frac{\pi}{N}\right]$ is absorbed in the fold. The shape of the other half of the petal ($-\pi/N \leq \theta \leq 0$) and of the other petals is obtained by symmetry.

The shape of the liquid interface is determined numerically using the software "Surface Evolver" (as described in the Methods section). For a given volume V, number of petals N and

DOI: 10.1038/NMAT4397

wrapping ratio ω, the shape of the interface of minimal area is determined; its area is the energy of the configuration. Then, the energy is minimized as a function of ω, and then as a function of N, to give the solid red line of Fig. 3. The best number of sides as a function of the size ratio W/R is plotted as black triangles and solid line in Fig. 4F.

2.3 Perturbation of the axisymmetric shape

We have also performed a calculation to test the stability of the axisymmetric shape to the introduction of a small fold. For any wrapping ratio ω, the polygonal shape converges to the axisymmetric shape when the number of folds N goes to infinity. As a consequence, a polygonal shape with a large number of folds can be seen as a perturbation of the axisymmetric shape, with $\epsilon = \pi/N$ as the small parameter. The stability of the axisymmetric shape against folding can then be investigated by looking at the derivative of the energy with respect to ϵ. This stability analysis would determine if there exists a finite critical threshold $(W/R)_c$ where the wrinkle-to-fold transition occurs.

The partial polygonal wrapping gives an exact construction for the shape of the sheet. However, a numerical analysis suggests that the effect of a small fold on the liquid interface is not local. As a consequence, an analysis of the stability of the axisymmetric shape to folding awaits a full description of the liquid interface.

3 Wrapping with a non-circular sheet

We have focussed our attention on the folding and symmetry-breaking behaviors of a circular sheet wrapping a drop. Here we show that by simply changing the shape of the sheet, the obtained wrappings can be significantly altered. Figure S4 shows a rectangular PS sheet of thickness $t = 113$ nm, with an aspect ratio of length to width of 6.5, placed on a water drop immersed in silicone oil. As before, we reduce the volume of the drop through a needle to

explore the wrapping shapes. At first, the sheet curls along its length, adopting a radius of curvature to match the approximately spherical drop. When the drop is small enough, the two short edges of the sheet meet, forming a ring around the drop, as shown in Fig. S4C. When the volume of the drop is reduced further, the sheet buckles in several locations along its two long edges (Fig. S4D). This buckling transition is shown in Movie S3.

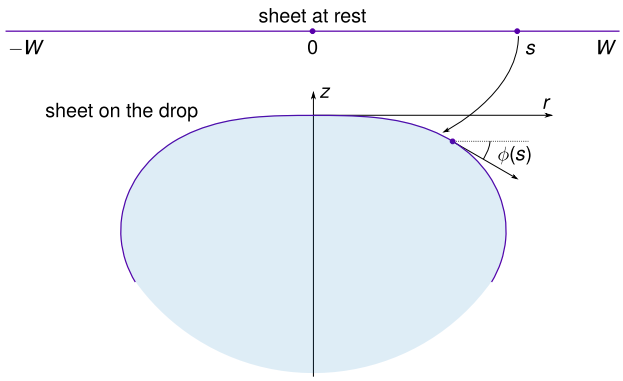

Figure S1: Sheet at rest (top) and adsorbed to the drop surface (bottom). The shape is obtained by revolution around the z axis. s is the material coordinate corresponding to the distance to the center of the sheet in the rest state.

DOI: 10.1038/NMAT4397

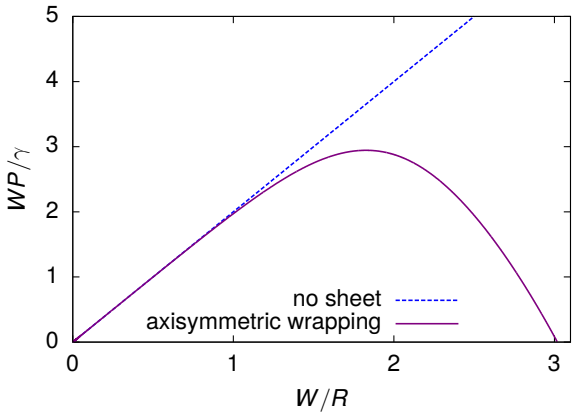

Figure S2: **Non-dimensional pressure inside an axisymmetrically-wrapped drop.** For small W/R (i.e., when the drop is much larger than the sheet), the presence of the sheet has little effect on the curvature of the fluid interface, and therefore the pressure is nearly equal to the value for a spherical drop with no sheet (dashed line). As the volume is reduced (increasing W/R), the pressure reaches a maximum and then decreases until it vanishes exactly at complete axisymmetric wrapping.

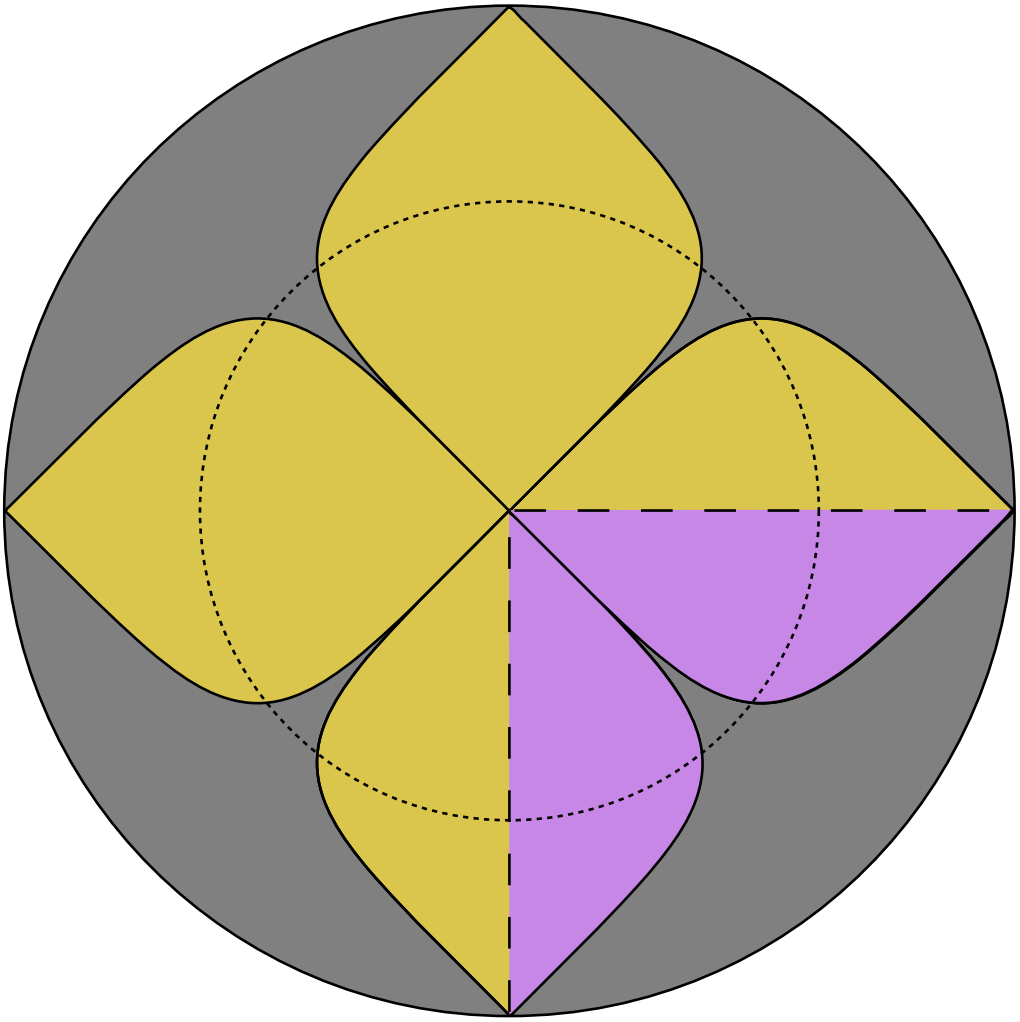

Figure S3: **Template for $n = 4$ polygonal partial or full wrapping.** To construct a full wrapping, print and cut out the entire disc, and fold along the curved edges of the four petals. For a partial wrapping, cut out a circular portion of the disc before folding.

DOI: 10.1038/NMAT4397

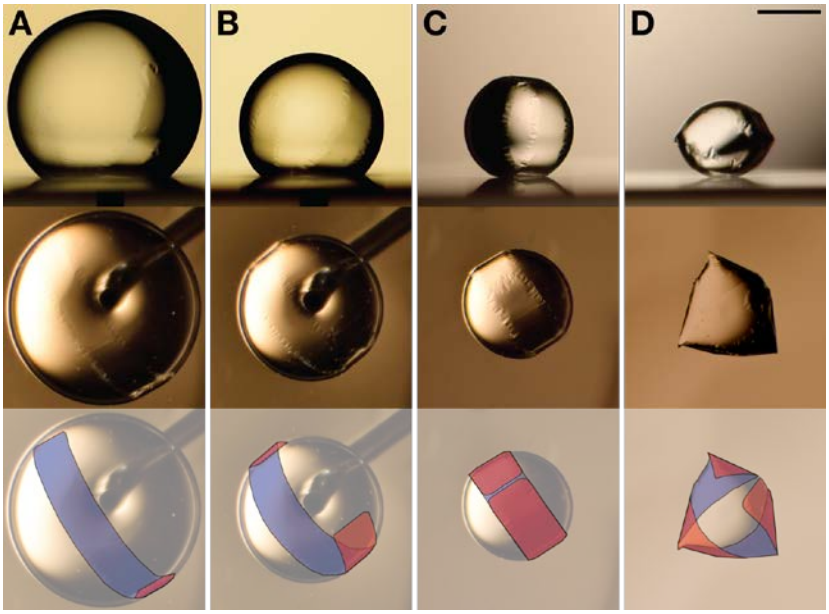

Figure S4: **Side and top views of a rectangular PS sheet wrapping a water drop immersed in silicone oil.** The sheet has thickness $t = 113$ nm, length 5.29 mm, and width 0.81 mm. (**A,B**) As the volume of the drop is decreased, the sheet conforms to the surface of the approximately spherical drop. (**C**) The sheet forms a ring around the drop when the short edges of strip meet. (**D**) Reducing the volume further, the sheet buckles at several points along its edge. Bottom row: schematics of the configuration of the sheet. Scale bar, 1 mm.

Captions for Movies S1 to S3:

Movie S1

Side view of a circular polystyrene sheet wrapping a water drop immersed in silicone oil. The sheet has thickness $t = 241$ nm and radius $W = 1.52$ mm. The drop sits on a layer of fluorinated oil, and its volume is controlled by a needle of diameter 0.4 mm inserted from below. Playback: $10\times$ real time. See Movie S2 for corresponding top view.

Movie S2

Top view of a circular polystyrene sheet wrapping a water drop immersed in silicone oil. The sheet has thickness $t = 241$ nm and radius $W = 1.52$ mm. The drop sits on a layer of fluorinated oil, and its volume is controlled by a needle of diameter 0.4 mm inserted from below. Playback: $10\times$ real time. See Movie S1 for corresponding side view.

Movie S3

Top and side views of a rectangular polystyrene sheet wrapping a water drop immersed in silicone oil. The sheet has thickness $t = 113$ nm, length 5.29 mm, and width 0.81 mm. The drop sits on a layer of fluorinated oil, and its volume is controlled by a needle of diameter 0.4 mm inserted from below. The movie shows the transition from an axisymmetric shape, where the sheet forms a ring around the drop, to a buckled configuration.